Journal of Medicinal Chemistry

Article

pubs.acs.org/jmc

Molecular Determinants of Ligand Binding Modes in the Histamine H_4 Receptor: Linking Ligand-Based Three-Dimensional Quantitative Structure−Activity Relationship (3D-QSAR) Models to in Silico Guided Receptor Mutagenesis Studies

Enade P. Istyastono,[†,§] Saskia Nijmeijer,[†,§] Herman D. Lim,[‡] Andrea van de Stolpe,[†] Luc Roumen,[†] Albert J. Kooistra,[†] Henry F. Vischer,[†] Iwan J. P. de Esch,[†] Rob Leurs,[†] and Chris de Graaf*[,†]

[†]Department of Pharmacochemistry, Faculty of Exact Sciences, Leiden/Amsterdam Center for Drug Research (LACDR), Division of Medicinal Chemistry, VU University Amsterdam, De Boelelaan 1083, 1081 HV Amsterdam, The Netherlands

[‡]Department of Medicinal Chemistry, Room P-246, Griffin Discoveries BV, De Boelelaan 1083, 1081 HV, Amsterdam, The Netherlands

S *Supporting Information*

ABSTRACT: The histamine H_4 receptor (H_4R) is a G protein-coupled receptor (GPCR) that plays an important role in inflammation. Similar to the homologous histamine H_3 receptor (H_3R), two acidic residues in the H_4R binding pocket, $D^{3.32}$ and $E^{5.46}$, act as essential hydrogen bond acceptors of positively ionizable hydrogen bond donors in H_4R ligands. Given the symmetric distribution of these complementary pharmacophore features in H_4R and its ligands, different alternative ligand binding mode hypotheses have been proposed. The current study focuses on the elucidation of the molecular determinants of H_4R−ligand binding modes by combining (3D) quantitative structure−activity relationship (QSAR), protein homology modeling, molecular dynamics simulations, and site-directed mutagenesis studies. We have designed and synthesized a series of clobenpropit (*N*-(4-chlorobenzyl)-*S*-[3-(4(5)-imidazolyl)propyl]isothiourea) derivatives to investigate H_4R−ligand interactions and ligand binding orientations. Interestingly, our studies indicate that clobenpropit (**2**) itself can bind to H_4R in two distinct binding modes, while the addition of a cyclohexyl group to the clobenpropit isothiourea moiety allows VUF5228 (**5**) to adopt only one specific binding mode in the H_4R binding pocket. Our ligand-steered, experimentally supported protein modeling method gives new insights into ligand recognition by H_4R and can be used as a general approach to elucidate the structure of protein−ligand complexes.

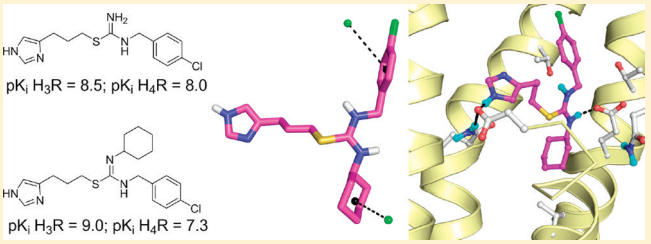

INTRODUCTION

The discovery of the human histamine H_4 receptor (H_4R) in 2000 has attracted attention from pharmaceutical industry and academia because the receptor plays an important role in allergic and inflammatory processes.[1−5] Together with the histamine H_1 (H_1R), H_2 (H_2R), and H_3 (H_3R), the H_4R belongs to the G protein-coupled histamine receptor family.[2,6−9] The H_4R shows a sequence identity at the protein level of 23%, 22%, and 31% with H_1R, H_2R, and H_3R, respectively.[1,6] Moreover, the putative histamine (**1**) binding pockets of H_3R and H_4R share a sequence identity of 56% and sequence similarity of ∼80%, explaining why the ligand pharmacophores for both receptors are very similar.[10] Some of the first H_4R ligands were previously known as selective H_3R ligands, e.g., **2** (clobenpropit) and **3** (imetit) (Figure 1).[1,2,6−9] Both H_3R and H_4R ligands typically have two hydrogen bond donors,[1,10] complementary with two negatively residues in the putative binding pocket of H_3R and H_4R, $D^{3.32}$ and $E^{5.46}$ (Ballesteros−Weinstein numbering).[1,11,12] These symmetric distributions of complementary pharmacophore features in the ligands and cavities of H_3R and H_4R make the definition of a ligand binding mode challenging, as previously demonstrated for **1**,[12−14] **2**,[15,16] **4a** (immepip),[13] **4b** (iodoproxyfan),[16] and **5** (VUF5228)[15] (Figure 1).

In general, two classes of binding modes have been proposed: one where the imidazole moiety binds to $E^{5.46}$ (mode I)[12,13,15] and another where the imidazole moiety binds to $D^{3.32}$ (mode II).[13,14,16−18] Although several GPCR crystal structures have been solved in the past 3 years, including the related bioaminergic β_1 adrenergic (ADRB1), β_2 adrenergic (ADRB2), dopamine D3 (DRD3), and histamine H_1 (H_1R) receptors,[19−22] experimental structures of H_3R or H_4R are still lacking. Only by combination of experimental information on both the ligand (e.g., structure−activity relationships) and the protein target (e.g., site-directed mutagenesis studies), reliable structural models of protein−ligand complexes can be constructed.[23] In the current study we present clobenpropit and its analogues, dual active H_3R/H_4R ligands[24] containing two basic groups, as useful tools to identify and recognize the chemical properties and features that determine the binding mode of ligands in the H_4R binding pocket. We have previously described

Received: August 3, 2011
Published: October 17, 2011

ACS Publications © 2011 American Chemical Society

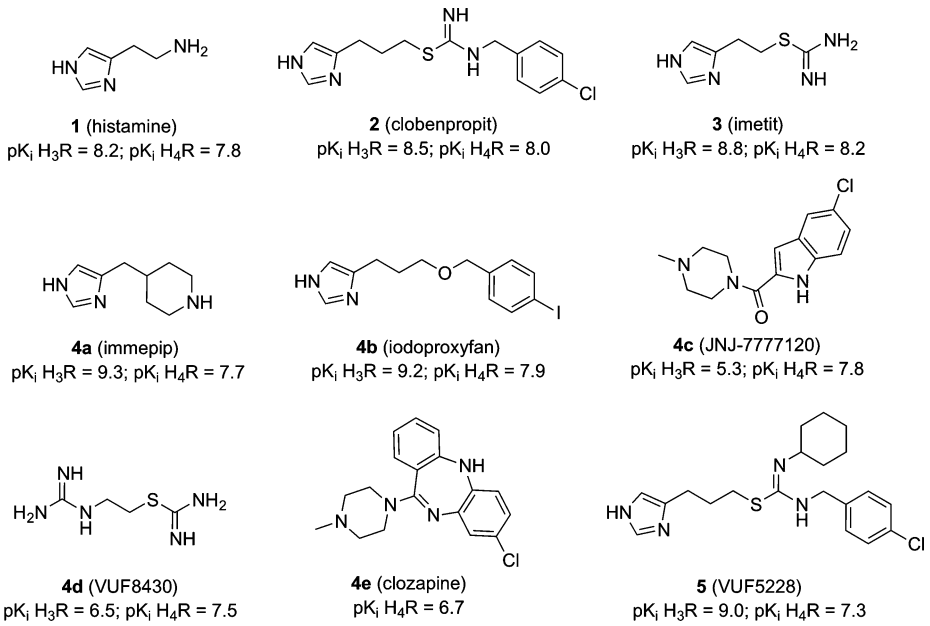

Figure 1. Structures of H_3R and H_4R ligands **1**−**5**. Biological activities are from refs 1 and 6 (**1**, **3**, **4**) and the current study (**2**, **5**).

quantitative structure−activity relationship (QSAR) studies on clobenpropit analogues that indicated that the stretch−bending energy (which depends on the conformation of the compounds) is an important property that explains the affinity of H_4R ligands.[24] This property also plays an important role in H_4R/H_3R selectivity. In order to better understand the importance of this descriptor, a new series of clobenpropit derivatives were synthesized and evaluated for their H_3R and H_4R affinity. Addition of a cyclohexyl moiety to compound **2** results in compound **5**, which has higher affinity for H_3R and much lower affinity for H_4R than **2** (Figure 1), resulting in a 16-fold increase in H_3R over H_4R selectivity. This additional lipophilic moiety is proposed to probe an additional lipophilic pocket in both H_3R[15,25] and H_4R.[1] By combining classical QSAR,[24] molecular interaction fields (MIF) based 3D-QSAR approaches,[26] and in silico guided site-directed mutagenesis (SDM) studies,[12,27,28] we were able to identify determinants of H_3R/H_4R selectivity and determine ligand binding modes in the H_4R binding pocket.

RESULTS AND DISCUSSION

The main aim of our study was to probe the important molecular features and residues that determine the binding orientation of ligands in the H_4R pocket. For this purpose, classical and three-dimensional (3D) quantitative structure−activity relationship (QSAR), protein homology modeling, molecular dynamics simulations, and site-directed mutagenesis (SDM) studies were combined in an integrative workflow (Figure 2) to investigate the binding modes of clobenpropit (**2**) and (*N*-(4-chlorobenzyl)-*S*-[3-(4(5)-imidazolyl)propyl]-isothiourea) clobenpropit analogues (**5** and **6**).

Design and Synthesis of Novel Clobenpropit (*N*-(4-Chlorobenzyl)-*S*-[3-(4(5)-imidazolyl)propyl]isothiourea) Derivatives. To probe the distinct hydrophobic pockets of the receptors, a series of compounds (**6a**−**l**) was designed and synthesized (Scheme 1). Intermediate 4-(3-bromo-propyl)-1*H*-imidazole hydrobromide (**7**), which was synthesized according to literature procedure,[29,30] was treated with thiourea compounds (**8a**−**l**). The corresponding thiourea compounds were prepared from commercially available isothiocyanates and the corresponding amines.

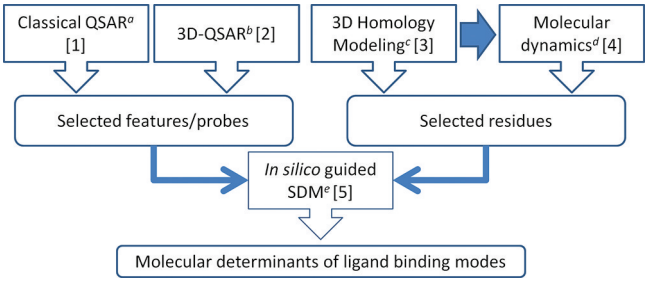

Figure 2. Flowchart of the approaches used in the current study. See Methods for more details. (a) SK-N-MC cells stably expressing H_3R or H_4R were used to determine ligand affinities for either the H_3R or the H_4R. The data were subjected to the classical QSAR method using MOE descriptors described previously[24] and (b) GRID MIF-based 3D-QSAR.[26,53] (c) PLANTS docking against H_3R and H_4R.[18,28] (d) Molecular dynamics simulations with AMBER.[38] (e) Site-directed mutagenesis (SDM) studies were performed as described previously.[12,28]

Addition of a Lipophilic Moiety Increases Selectivity toward H_3R. Compounds **2**, **5**, and **6a**−**l** were investigated for their H_3R and H_4R affinity (Table 1) and were subsequently subjected to QSAR studies. Addition of a cyclohexyl moiety to compound **2**, resulting in compound **5**, increases the H_3R affinity but decreases the H_4R affinity. Further investigation shows that smaller lipophilic substituents (compare **6a** to **6b**) decrease the H_3R affinity and slightly increase the H_4R affinity. Remarkably, a cyclopentyl substitution at R_1 results in a compound (**6a**) with similar affinity for both the H_3R and the H_4R ($\Delta pK_i = 0$). Among the series, only compounds **6c** and **6i** have a slightly favorable affinity toward the H_4R ($\Delta pK_i = -0.4$). These compounds are among the smallest compounds in the series. On the other hand, compound **6d**, one of the largest compounds, shows the highest H_3R selectivity over H_4R ($\Delta pK_i = 2.16$). This is in line with earlier (Q)SAR, indicating that steric properties play an important role in driving H_3R over H_4R selectivity.[13,24]

Steric QSAR Descriptors Determine the Activity of the Ligands to the H_3R and the H_4R. QSAR models to describe the binding of the ligands to both the H_3R (eq 1) and the H_4R

dx.doi.org/10.1021/jm201042n | J. Med. Chem. 2011, 54, 8136–8147

Scheme 1[a]

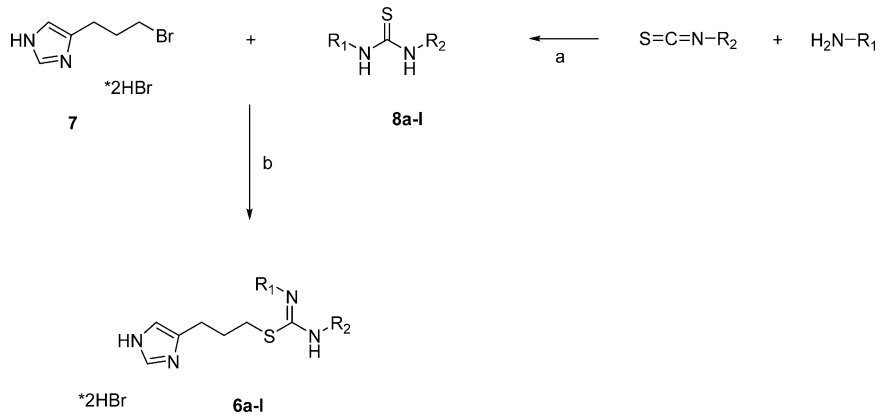

[a](a) Et_2O, room temp, 1 h; (b) ethanol, microwave, 120 °C, 0.5 h.

Table 1. Affinity (pK_i) of Clobenpropit Analogues at the Human H_3R and the Human H_4R

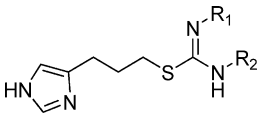

compd	R_1	R_2	$pK_i(H_3R)$ [a]	$pK_i(H_4R)$ [a]	ΔpK_i [b]
2	H	4-chlorobenzyl	8.55 ± 0.08	8.00 ± 0.06	0.55
5	cyclohexyl	4-chlorobenzyl	8.98 ± 0.09	7.32 ± 0.14	1.66
6a	cyclopentyl	benzyl	7.37 ± 0.02	7.37 ± 0.02	0.00
6b	cyclohexyl	benzyl	8.01 ± 0.05	7.12 ± 0.03	0.89
6c	cyclopentyl	*n*-butyl	7.33 ± 0.07	7.79 ± 0.01	−0.46
6d	3,4-dichlorobenzyl	cyclohexyl	8.99 ± 0.11	6.83 ± 0.10	2.16
6e	4-chlorobenzyl	*n*-butyl	8.31 ± 0.08	7.05 ± 0.01	1.26
6f	4-chlorobenzyl	benzyl	7.77 ± 0.04	6.64 ± 0.09	1.13
6g	3,4-dichlorobenzyl	benzyl	7.49 ± 0.13	6.42 ± 0.10	1.07
6h	cyclopentyl	cyclohexyl	7.73 ± 0.10	7.50 ± 0.04	0.23
6i	cyclopentyl	*tert*-butyl	7.17 ± 0.09	7.53 ± 0.08	−0.36
6j	3,4-dichlorobenzyl	*n*-butyl	8.33 ± 0.10	7.05 ± 0.09	1.28
6k	4-cyanobenzyl	cyclohexyl	8.79 ± 0.10	6.90 ± 0.07	1.89
6l	4-nitrobenzyl	cyclohexyl	8.94 ± 0.10	6.87 ± 0.05	1.88

[a]SK-N-MC cells stably expressing H_3R or H_4R were used to determine ligand affinities for either the H_3R or the H_4R. Data shown are the mean ± SEM of at least three independent experiments. [b]$\Delta pK_i = pK_i(H_3R) - pK_i(H_4R)$.

(eq 2) were generated, using a similar approach as reported previously.[24] Equation 1 shows that the ligand affinity to the H_3R is determined by a steric descriptor (Diameter) and a combined steric−electronic descriptor (BCUT_SMR_0),[31,32] while eq 2 shows that ligand affinity at H_4R is determined by solely steric descriptors (vdw_area and E_strain). Interestingly, similar to the previous QSAR studies,[24,32] an energy-related descriptor (E_strain) emerges as the important descriptor describing the ligand affinity to the H_4R. Both descriptors (E_stb in the previous QSAR studies and E_strain in this study) are conformation-related descriptors, and E_stb was proposed as the selectivity determining descriptor.[24,32] This indicates that clobenpropit analogues bind to the H_4R binding pocket in an energetically less favorable conformation than in the H_3R binding pocket.[33]

$$pK_i(H_3R) = (-3.815 \pm 1.960) + (0.410 \pm 0.075)[\text{Diameter}] - (2.668 \pm 0.737)[\text{BCUT\_SMR\_0}] \quad (1)$$

$$N = 14, \quad r = 0.900, \quad R^2 = 0.810, \quad S = 0.312, \quad F = 23.454, \quad F_{5\%,2,11} = 3.982, \quad q^2 = 0.699$$

$$pK_i(H_4R) = (12.495 \pm 0.314) - (0.014 \pm 0.001)[\text{vdw\_area}] - (0.014 \pm 0.003)[\text{E\_strain}] \quad (2)$$

$$N = 14, \quad r = 0.984, \quad R^2 = 0.968, \quad S = 0.085, \quad F = 166.751, \quad F_{5\%,2,11} = 3.982, \quad q^2 = 0.949$$

Linking Steric Descriptors to 3D-QSAR Hydrophobic Probes. In order to correlate the information regarding important global ligand features (step 1 in Figure 2) to ligand−receptor binding modes in three-dimensional space, 3D-QSAR models (step 2 in Figure 2) were constructed correlating molecular interaction fingerprints (MIFs)[26] with H_3R (eq 3) and H_4R (eq 4) ligand binding affinities. The structure of **5** was generated using CORINA, resulting in two 3D configurations (Figure 3).[34] Ab

dx.doi.org/10.1021/jm201042n | J. Med. Chem. 2011, 54, 8136–8147

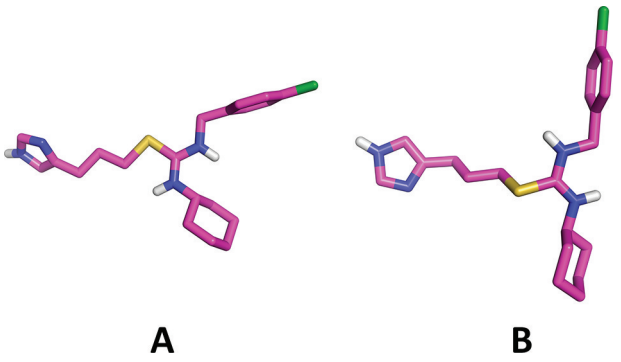

Figure 3. Depiction of two configurations of compound **5** generated with CORINA.

initio (DFT/6-31G*) optimizations with Gaussian were performed for both 3D configurations.[35−37] The lower energy configuration suggested by the ab initio calculations (Figure 3B) was selected as the reference structure to align **2** and **6a−l** with ROCS to construct MIF-based 3D-QSAR models (Figure 4).[38,39] Interestingly, a hydrophobic probe (DRY.1) and a polar probe (O.1) are descriptors in the H_3R 3D-QSAR model (eq 3, Figure 4A), which correspond to the steric (Diameter) and steric−electronic (BCUT_SMR_0) descriptors in the classical H_3R QSAR model (eq 1). The single hydrophobic descriptor (DRY.2) in the H_4R 3D-QSAR model (eq 4, Figure 4B), on the other hand, matches the steric descriptors (vdw_area and E_strain) in the classical H_4R QSAR model (eq 2).

$$pK_i(H_3R) = (7.975 \pm 0.163) + (0.287 \pm 0.039)[\text{DRY.1}] + (0.209 \pm 0.057)[\text{O.1}] \quad (3)$$

$$N = 14, \quad r = 0.930, \quad R^2 = 0.865, \quad S = 0.263, \quad F = 35.377, \; F_{5\%,2,11} = 3.982, \quad q^2 = 0.785$$

$$pK_i(H_4R) = (7.947 \pm 0.076) + (0.232 \pm 0.020)[\text{DRY.2}] \quad (4)$$

$$N = 14, \quad r = 0.958, \quad R^2 = 0.917, \quad S = 0.132, \quad F = 132.877, \quad F_{5\%,1,12} = 4.750, \quad q^2 = 0.891$$

Since the (3D-)QSAR models (eqs 1−4) models indicated an important role of steric/hydrophobic descriptors in determining H_3R and H_4R affinity, a 3D-QSAR model predicting the difference between H_4R and H_3R affinity (ΔpK_i) was constructed. The result (eq 5) reveals two hydrophobic probes that determine H_3R over H_4R selectivity, one that is within 3.8 Å from the hydrophobic centroid of the cyclohexyl moiety (DRY.4) of compound **6** (Figure 4C). Another selectivity determining probe is located within 3.9 Å from the hydrophobic centroid of

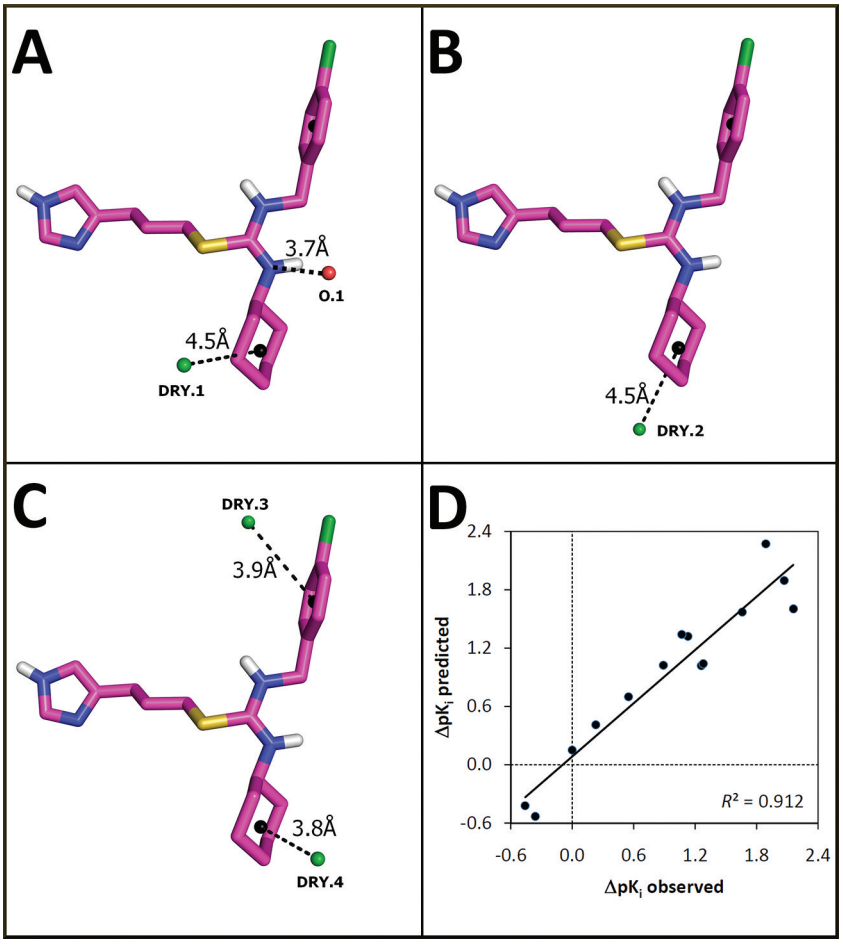

Figure 4. Structure of compound **5** in 3D with important probes explaining the ligand affinity to H_3R (eq 3, A), important probes explaining the ligand affinity to H_4R (eq 4, B), and important probes explaining the H_3R/H_4R selectivity (eq 5, C). The distances between hydrophobic probes to the nearest hydrophobic centroid of compound **6** (presented as black spheres) are presented in parts A−C. Graph between observed and calculated ΔpK_i is presented in part D.

dx.doi.org/10.1021/jm201042n | J. Med. Chem. 2011, 54, 8136−8147

the aromatic moiety (DRY.3) of compound **6** (Figure 4C).

$$\Delta pK_i = pK_i(H_3R) - pK_i(H_4R)$$
$$= (-0.664 \pm 0.171) - (0.126 \pm 0.018)$$
$$[DRY.3] - (0.112 \pm 0.025)[DRY.4] \quad (5)$$

$$N = 14, \quad r = 0.955, \quad R^2 = 0.912, \quad S = 0.277,$$
$$F = 57.249, \quad F_{5\%,2,11} = 3.982, \quad q^2 = 0.862$$

The descriptors used in the (3D-)QSAR models (eqs 1−5) are described in Table 2. All models have acceptable statistical significances (N = number of samples, F = test for quality of fit, r = coefficient of correlation, R^2 = coefficient of determination, S = standard error of estimation, and q^2 = leave-one-out cross-validation).[24,40] Moreover, a total of 1000 runs of Y-randomization was performed for each model to show the distribution of the dependent variable values. The results show that the internal predictivity (q^2) of each model was better than any of the 1000 scrambled models. We are therefore confident that the number of examples is sufficient and heterogeneous.[24,41]

Table 2. Definition of the Descriptors in the QSAR Models (Eqs 1−5)

descriptor[a]	definition
Diameter	largest value in the distance matrix
BCUT_SMR_0	the BCUT descriptors using atomic contribution to molar refractivity[31,32,61]
vdw_area	area of van der Waals surface calculated using a connection table approximation
E_strain	local strain energy
DRY.1	interaction energy value of hydrophobic probe DRY.8331 (4.0, −1.0, 2.0)
O.1	interaction energy value of sp^2 carbonyl oxygen probe O.6874 (7.0, −6.0, 1.0)
DRY.2	interaction energy value of hydrophobic probe DRY.8195 (−2.0, −5.0, 2.0)
DRY.3	interaction energy value of hydrophobic probe DRY.3376 (9.,; −6.0. −8.0)
DRY.4	interaction energy value of hydrophobic probe DRY.9361 (5.0, −5.0, 4.0)

[a]Descriptors diameter, BCUR_SMR_0, vdw_area, and E_strain generated with the QuaSAR descriptor module in MOE.[24,32] Interaction energy values of GRID[26,53] interaction points DRY.8331 (DRY.1), O.6874 (O.1), DRY.8195 (DRY.2), DRY.3376 (DRY.3), and DRY.9361 (DRY.4) at specific positions (Cartesian coordinates from the midpoint of compound **6**).

Linking QSAR Studies to 3D Homology Models. In parallel with the synthesis, pharmacological evaluation, and the QSAR modeling of clobenpropit analogues as dual active H_3R and H_4R ligands, ADRB2-based[19] homology models of H_4R (step 3 in Figure 2) were generated to identify the selectivity determining residues. These residues were subsequently investigated by site-directed mutagenesis studies to elucidate the binding modes of compounds **2** and **5** in the H_4R binding pocket. Compounds **2** and **5** have two moieties, imidazole and isothiourea moieties, that can act as hydrogen bond donors to interact with the receptor.[1,15,24,25] The H_4R binding pocket has two residues, $D^{3.32}$ and $E^{5.46}$, that have been shown to be essential for ligand binding[1,12,28,42] and are proposed to act as complementary negatively ionizable hydrogen bond acceptors. A similar phenomenon is observed in the recently solved CXC chemokine receptor 4 (CXCR4) crystal structure, where the two small molecule antagonist 1T forms ionic interactions with $D^{2.63}$ and $E^{7.39}$ via its imidazole and isothiurea groups, respectively.[43,44] The recent GPCR DOCK 2010 challenge demonstrated that this symmetric distribution of complementary pharmacophore features in ligand and protein made the prospective prediction of CXCR4−ligand interactions highly challenging.[45,46] In line with the same philosophy we followed in our successful CXCR4−ligand binding pose prediction in this community wide GPCR modeling assessment,[44] we investigated two putative H_4R binding mode hypotheses: one where the imidazole moiety binds to $E^{5.46}$ (mode I, i.e., models in Figure 5A and Figure 5C)[12,13,15] and another where the imidazole moiety binds to $D^{3.32}$ (mode II, i.e., in Figure 5B and Figure 5D).[13,14,16,17]

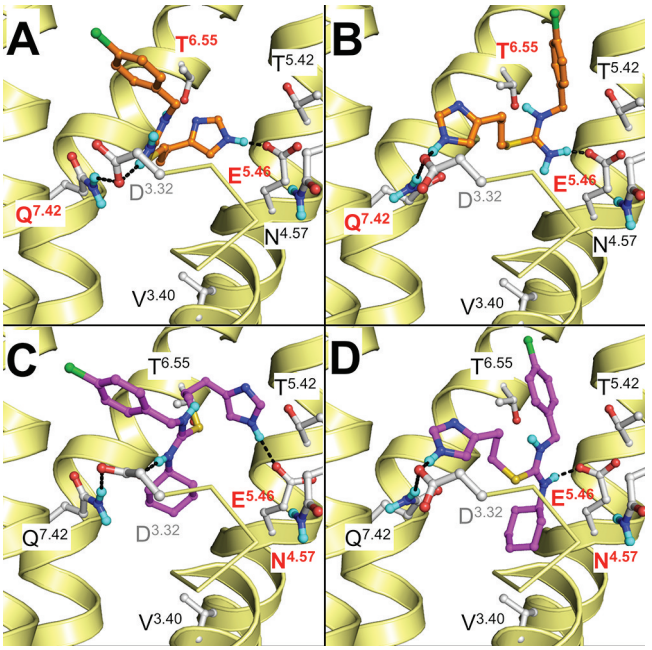

Figure 5. Possible binding modes of compounds **2** (A, B) and **5** (C, D) in the H_4R 3D homology models.[1] Compound **2** is depicted as ball-and-sticks with orange carbon atoms, while compound **5** is depicted with magenta carbon atoms. The backbones of TM helices 4, 5, 6, and 7 are represented by yellow ribbons, and part of TM3 is shown as ribbon (the top of the helix is not shown for clarity). Important binding residues are depicted as ball-and-sticks with gray carbon atoms. Residues studied by side-directed mutagenesis are labeled (note that $D^{3.32}$ has not been mutated in the current study but has previously been shown to be an essential residue for H_4R ligand binding[1,11,12] and is labeled in gray). If the K_i of the point mutant for the specific ligand is decreased by 5-fold or more (compared to the K_i of wild type H_4R), the residue is labeled red.

The hydrogen bond network with $D^{3.32}$ (an essential H_4R hydrogen bond anchor as determined by previous SDM)[1,28,42,47] was further investigated by molecular dynamics (MD) simulations (step 4 in Figure 2). Analysis of the MD trajectories (Supporting Information Table 5) showed that the H-bond network between $D^{3.32}$ and **2** remained stable in both binding modes I (observed in 99% of the MD snapshots, starting from the structure in Figure 5A) and II (observed in 97% of the snapshots, starting from the structure in Figure 5B). Compound **5**, however, only formed a stable H-bond with $D^{3.32}$ in binding mode II (observed in 99% of the MD snapshots, starting from the structure in Figure 5D). This suggests that binding mode II is the most plausible binding orientation for **5**, while **2** is able to adopt both binding modes I and II in the H_4R binding pocket.

dx.doi.org/10.1021/jm201042n | J. Med. Chem. 2011, 54, 8136−8147

By combining 3D-QSAR studies (Figure 4) and H_4R receptor modeling studies (Figure 5, Table 3), we proposed residues that might play an important role in H_4R-ligand binding. We hypothesized that residues responsible for H_3R/H_4R selectivity (Table 1) are H_4R specific (i.e., are different residues in H_3R) and match the essential interaction probes derived from our 3D-QSAR studies (i) within 4.5 Å from the hydrophobic centroid of the cyclohexyl moiety (Figure 4A and Figure 4B), (ii) within 3.9 Å from the hydrophobic centroid of the aromatic moiety (Figure 4C), or (iii) within 3.7 Å from the protonated nitrogen (Figure 4A). In this way, residue $Q^{7.42}$ is identified as a potential determinant of H_4R–ligand binding based on binding mode **I** (Figure 5A and Figure 5C), while residues $V^{3.40}$, $N^{4.57}$, $T^{5.42}$, and $T^{6.55}$ are selected based on binding mode II (Figure 5D and Figure 5D). We furthermore wanted to investigate the role of $D^{3.32}$ and $E^{5.46}$ as putative ionic/H-bond interaction anchors of **2** and **5** (Figure 5). Unfortunately, a suitable $D^{3.32}$ mutant to study radioligand displacement is not available because mutation of this residue is detrimental to binding of both histamine (**3**) and JNJ-7777120 (5-chloro-2-[(4-methylpiperazin-1-yl)carbonyl]-1*H*-indole, **4c**).[12] Our H_4R models, however, suggest that $Q^{7.42}$ forms an intramolecular H-bond with $D^{3.32}$ (Figure 5) and might indirectly modulate ligand interactions with this residue. The previously reported H_4R $E^{5.46}Q$ mutant has interesting ligand dependent effects on binding affinity[12,42] and was therefore selected to study the role of the negatively ionizable $E^{5.46}$ in binding of **2** and **5**.

Table 3. The affinity (pK_i) of 1 and 6 at the human H_3R[a], the human H_4R[b], and some H_4R mutants[c]

Mutant	pK_i[d]	
	2	5
H_3R WT	9.2 ± 0.14	9.3 ± 0.34
H_4R WT	8.1 ± 0.08	7.5 ± 0.11
H_4R $V^{3.40}A$	8.0 ± 0.07	7.2 ± 0.08
H_4R $N^{4.57}Y$	7.8 ± 0.07	6.5 ± 0.05
H_4R $T^{5.42}A$	8.6 ± 0.13	7.9 ± 0.15
H_4R $E^{5.46}Q$	7.3 ± 0.10	6.8 ± 0.07
H_4R $T^{6.55}M$	8.8 ± 0.08	7.9 ± 0.19
H_4R $Q^{7.42}L$	9.0 ± 0.17	7.9 ± 0.14

[a]Measured by displacement of [^{3}H]*N*-α-methylhistamine binding using membranes of HEK293T cells transiently expressing the human H_3R. [b]Measured by displacement of [^{3}H]histamine binding using membranes of HEK293T cells transiently expressing either the human H_4R or the H_4R mutants. [c]H_4R-$E^{5.46}Q$ data were obtained by displacement of [^{3}H]-JNJ-7777120 (tritiated **4c**). [d]Data shown are mean ± SEM of at least three independent experiments.

In Silico Guided Site-Directed Mutagenesis Studies Identify Molecular Determinants of H_3R/H_4R Selectivity and Elucidate Ligand Binding Modes in H_4R. Our integrative ligand-based 3D-QSAR and protein-based H_4R modeling approach was used to design site-directed mutagenesis studies to elucidate the binding mode of clobenpropit and its analogues in H_4R (step 5 in Figure 2). Table 3 shows the binding affinities of **2** and **5** at the $E^{5.46}Q$ mutant and the five H_4R mutants mimicking the H_3R binding pocket ($V^{3.40}A$, $N^{4.57}Y$, $T^{5.42}A$, $T^{6.55}M$, $Q^{7.42}L$).

The affinities of **2** and **5** at the $E^{5.46}Q$ mutant compared to H_4R WT are decreased by about 6-fold (Table 4, Figure 6A,B). Interestingly, the same mutation results in an even larger decrease in the affinity for small ligands containing two basic groups (**1** and **4d** (VUF8430)) but does not affect the binding affinity of the larger hydrophobic ligands with one basic moiety (**4c** and **4f** (clozapine)).[12,42] Apparently, **2** and its analogue **5**,

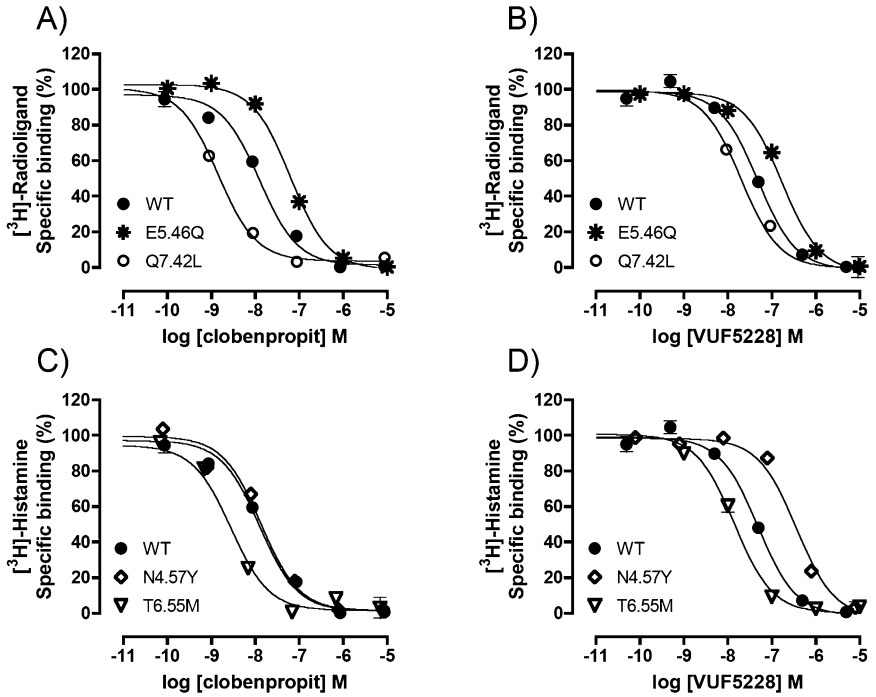

Figure 6. Radioligand displacement curves of compound **2** (A, C) and compound **5** (C, D) on a selected set of indicated H_4R mutants $E^{5.46}Q$ (∗); $Q^{7.42}L$ (○); $N^{4.57}Y$ (◇); $T^{6.55}$ M (▽) and WT (●). $E^{5.46}Q$ mutant data were determined with [^{3}H]JNJ-7777120 radioligand, whereas [^{3}H]histamine was used for H_4R WT and all other H_4R mutants. Data shown are representative specific binding curves of at least three experiments performed in triplicate. Error bars indicate SEM values. To enable a better visualization of the pK_i shifts, each curve is corrected for the radioligand concentration and the K_d for WT or mutant H_4Rs.

dx.doi.org/10.1021/jm201042n | J. Med. Chem. 2011, 54, 8136–8147

which also contain two basic groups but are relatively larger and more hydrophobic than **3** and **4d**, depend only partly on ionic interactions with $E^{5.46}$. The H_4R $Q^{7.42}L$ mutant has a significantly increased affinity for **2** (9-fold compared to H_4R WT), resulting in pK_i comparable to that for H_3R, but has a much smaller (2-fold) effect on the affinity of **5** (Table 3, Figure 6A,B). This residue, which was identified by probe O.1 in 3D-QSAR studies (Figure 4A; step 2 in Figure 2) and homology modeling (Figure 5A and Figure 5C), acts as a clear selectivity switch for **2**.

Similar to the H_4R $Q^{7.42}L$ mutation, the $T^{6.55}$ M mutation has a larger effect on the affinity for **2** than for **5** (Table 3, Figure 6C,D). Residues $T^{5.42}$ and $T^{6.55}$ were identified by probe DRY.3 in 3D-QSAR studies (Figure 3C) and 3D homology models (Figure 5B and Figure 5D). Since the H_4R $T^{6.55}$ M mutant shows more pronounced effect in determining H_3R selectivity toward H_4R compared to H_4R $T^{5.42}A$ mutant, we propose that DRY.3 matches residue $T^{6.55}$. Interestingly, the $N^{4.57}Y$ mutation significantly reduces the affinity of **5** by 10-fold but only slightly affects the affinity of **2** (Table 3, Figure 6C,D). The residue at position 4.57 has been shown to be an important molecular determinant of H_4R species differences in ligand binding.[28] In pig and dog H_4R the $H^{4.57}$ residue is proposed to influence the orientation of $E^{5.46}$ by forming direct H-bond interactions.[28] We postulate the same mechanism for the $N^{4.57}Y$ mutant and hypothesize that the larger $Y^{4.57}$ residue fixes the orientation of the $E^{5.46}$ side chain in a way that is not compatible with the binding mode of **5** in the H_4R pocket. While clobenpropit can adopt the position of its imidazole (mode I) or isothiurea (mode II) group to this alternative orientation of $E^{5.46}$, the binding orientation of clobenpropit analogue **5** is relatively rigid because of its bulky cyclohexyl group which binds deep in the hydrophobic pocket between TM3, TM4, TM5, and TM6 (Figure 5). The $N^{4.57}$ residue was identified by probes DRY.2 and DRY.4 in the 3D-QSAR studies (Figure 4B and Figure 4C) based on binding mode II (Figure 5B and Figure 5D). The H_4R $V^{3.40}A$ mutant was studied, since it was indicated by similar probes identifying residue $N^{4.57}$. However, despite the fact that the residue in position 3.40 is a determinant in H_3R species differences and influences H_1R activation,[48−50] the $V^{3.40}A$ mutant has almost no effect on the affinity of **2** and **5** (Table 3). Therefore we propose that probes DRY.2 and DRY.4 in the 3D-QSAR studies (Figure 4B and Figure 4C) pinpoint residue $N^{4.57}$ as a determinant of H_3R/H_4R selectivity for this compound.

In conclusion, while binding of compound **2** to H_4R is affected by mutation of the $Q^{7.42}$ residue (corresponding binding mode I in Figure 5A) and by mutation of the $T^{6.55}$ residue identified (corresponding with binding mode II in Figure 5B), binding affinity of **5** for H_4R is only significantly affected by mutated residue $N^{4.57}$ (corresponding with binding mode **II** in Figure 5D). Therefore, we propose that compound **2** can adopt two different binding modes (I and II) in the H_4R binding pocket, while **5** only adopts binding mode II. These data are furthermore in line with our molecular dynamics studies (Supporting Information Table 5), indicating that **5** can only form a stable H-bond network with $D^{3.32}$ in this binding orientation. An alternative explanation for the role of $Q^{7.42}$ in clobenpropit binding is that it modulates the clobenpropit binding orientation by forming an intramolecular H-bond with the essential $D^{3.32}$ residue. The binding mode of **5** is more rigid because its bulky cyclohexyl group binds in the hydrophobic pocket between TM3, 5, and 6 (Figure 5D) and is therefore less affected by the $Q^{7.42}L$ mutation.

CONCLUSIONS

By combining ligand-based QSAR models, protein-based H_4R modeling studies, and in silico guided site-directed mutagenesis experiments, we have systematically identified the molecular determinants that drive H_3R/H_4R selectivity and used this information to elucidate the binding modes of clobenpropit (**2**) and its analogues (**5**, **6**) in the H_4R binding pocket. QSAR studies on a novel series of clobenpropit derivatives containing two lipophilic moieties indicated that descriptors related to ligand size and conformation energy were correlated with H_4R binding affinity and identified molecular interaction probes that drive H_3R over H_4R selectivity. Linking these essential 3D-QSAR probes to specific residues in H_4R receptor models enabled the design of site-directed mutagenesis studies to elucidate H_4R−ligand binding modes. Our studies indicate that clobenpropit (**2**) can adopt two distinct binding modes in H_4R, while the addition of a cyclohexyl group to the clobenpropit isothiourea moiety allows compound **5** to adopt only one specific binding orientation in the H_4R binding cavity. Our experimentally supported ligand-steered protein modeling method gives new insights into ligand recognition by H_4R and can be used as a general approach to elucidate the structure of protein−ligand complexes.

METHODS

Synthetic Methods. Chemicals were obtained from commercial suppliers and were used without further purification. ^1H NMR and ^{13}C NMR spectra were recorded on a Bruker AC-200 (200 MHz) spectrometer or a Bruker Avance 400 (400 MHz) spectrometer. Microwave assisted chemistry was performed with a Biotage Initiator typically using 2 or 5 mL vials obtained from Biotage (Sweden). Purity of the synthesized compounds **2**, **5**, and **6a−l** was verified to be at least 95% by liquid chromatography−mass spectrometry (LCMS, see Supporting Information Table 1). LCMS analyses were performed with a Shimadzu LCMS-2010 EV mass spectrometer, a Shimadzu LC-20 AB pump system, a SPD-M20 A diode array detector, and a CTO-20 AC column oven using an XBrigde column (C18, 5 μm, 4.6 mm × 50 mm). An aqueous buffer (pH 8) of 0.04% NH_4HCO_3 (solvent A) and a mixture of 90% MeCN and 10% of a 0.4% NH_4HCO_3 buffer (pH 8, solvent B) were used. The runs started with 5% B with a linear gradient to 90% B in 4.5 min, then continuing for 1.5 min with 90% B and finally a linear gradient to 5% B in 0.5 min. Total run time was 8 min. J. T. Baker silica gel was used for flash chromatography. All melting points are uncorrected and were measured on an Optimelt automated melting point system from Stanford Research Systems.

General Method A. The following procedure was used to obtain the intermediate thiourea compounds **8a−l**. A solution of 30 mmol of the amine in 20 mL of diethyl ether was added dropwise to a solution of 30 mmol of the isothiocyanate in 25 mL of diethyl ether. The reaction mixture was stirred for 1 h. The precipitated product was filtered off and washed 3 times with diethyl ether. Isolated yields are between 85% and 95%.

*1-Benzyl-3-cyclopentylthiourea (**8a**).* ^1H NMR($CDCl_3$): δ 1.34−1.75 (m, 6H); 1.82−2.08 (m, 2H); 4.07 (bs, 1H); 4.69 (d, J = 4.97 Hz, 2H); 5.91 (bs, 2H).

*1-Benzyl-3-cyclohexylthiourea (**8b**).* ^1H NMR ($CDCl_3$): δ 1.01−1.41 (m, 5H); 1.48−1.75 (m, 4H); 1.95 (d, J = 11.83 Hz, 2H); 3.80 (bs, 1H); 4.62 (d, J = 4.94 Hz, 2H); 5.68 (bs, 1H); 6.00 (bs, 1H); 7.28−7.35 (m, 5H).

*1-Butyl-3-cyclopentylthiourea (**8c**).* ^1H NMR ($CDCl_3$): δ 0.92 (t, J = 7.2 Hz, 3H); 1.20−1.80 (m, 10H); 1.95−2.15 (m, 2H); 3.43 (m, 2H); 4.10 (bs, 1H); 5.62 (bs, 1H); 5.80 (bs, 1H).

*1-Cyclohexyl-3-(3,4-dichlorobenzyl)thiourea (**8d**).* ^1H NMR ($CDCl_3$): δ 1.11−1.40 (m, 5H); 1.50−1.76 (m, 3H), 1.90−1.99 (m, 2H); 3.73 (bs, 1H); 4.66 (d, J = 5.57 Hz, 2H); 5.89 (bs, 1H); 6.12 (bs, 1H); 7.12 (dd, J_1 = 6.25 Hz, J_2 = 1.95 Hz, 1H); 7.31−7.42 (m, 2H).

*1-Butyl-3-(4-chlorobenzyl)thiourea (**8e**).* ^{1}H NMR ($CDCl_3$): δ 0.88 (t, J = 7.18 Hz, 3H); 1.30 (s, 2H), 1.50 (dd, J_1 = 7.6 Hz, J_2 = 6.87 Hz, 2H); 3.30 (bs, 2H); 4.64 (d, J = 5.29 Hz, 2H); 5.84 (bs, 1H); 6.00 (bs, 1H); 7.21−7.32 (m, 4H).

*1-Benzyl-3-(4-chlorobenzyl)thiourea (**8f**).* ^{1}H NMR ($CDCl_3$): δ 4.57 (d, J = 6.67 Hz, 2 h); 4.60 (d, J = 5.94 Hz, 2H); 6.00 (bs, 1H); 6.15 (bs, 1H), 7.08−7.40 (m, 9H).

*1-Benzyl-3-(3,4-dichlorobenzyl)thiourea (**8g**).* ^{1}H NMR ($CDCl_3$): δ 4.56 (d, J = 5.25 Hz, 2H); 4.65 (d, J = 5.65 Hz, 2H); 5.97 (bs, 1H); 6.25 (bs, 1H); 7.02 (dd, J_1 = 8.12 Hz, J_2 = 0 Hz, 1 h); 7.12−7.48 (m, 7H).

*1-Cyclohexyl-3-cyclopentylthiourea (**8h**).* ^{1}H NMR ($CDCl_3$): δ 1.04−1.78 (m,16H); 1.82−2.12 (m, 2H); 4.03 (bs, 2H); 5.53 (bs, 1H); 5.83 (bs, 1H).

*1-(tert-butyl)-3-cyclopentylthiourea (**8i**).* ^{1}H NMR ($CDCl_3$): δ 1.39 (s, 10H); 1.40−1.73 (m, 7H); 1.94−2.16 (m, 2H); 4.35 (bs, 1H); 5.64 (bs, 1H); 5.84 (bs, 1H).

*1-Butyl-3-(3,4-dichlorobenzyl)thiourea (**8j**).* ^{1}H NMR ($CDCl_3$): δ 0.87 (t, J = 7.1 Hz, 3H); 1.30 (m, J_1 = 8.09 Hz, J_2 = 7.02 Hz, J_3 = 7.15 Hz, 2H); 1.50 (q, J_1 = 3.75 Hz, J_2 = 7.43 Hz, 2H); 3.30 (bs, 2H); 4.65 (d, J = 5.57 Hz, 2H); 6.10 (bs, 1H); 6.28 (bs, 1H); 7.11 (dd, J_1 = 6.26 Hz, J_2 = 2.01 Hz, 1H); 7.34 (d, J = 2.98 Hz, 1H); 7.36 (d, J = 3.22 Hz, 1H).

*1-(4-Cyanobenzyl)-3-cyclohexylthiourea (**8k**).* ^{1}H NMR ($CDCl_3$, 200 MHz): δ 0.99−1.43 (m, 5H); 1.50−1.82 (m, 3H); 1.87−2.08 (m, 2H); 3.76 (bs, 1H), 4.78 (d, J = 5.68 Hz, 2H); 6.00 (bs, 1H); 6.33 (bs, 1H); 7.36 (d, J = 8.20 Hz, 2H); 7.51 (d, J = 8.30 Hz, 2H).

*1-Cyclohexyl-3-(4-nitrobenzyl)thiourea (**8l**).* ^{1}H NMR ($CDCl_3$): δ 1.04−1.47 (m, 5H); 1.52−1.82 (m, 3H); 1.83−2.08 (m, 2H); 3.71 (bs, 1H); 4.89 (d, J = 5.80 Hz, 2H); 5.89 (bs, 1H), 6.03 (bs, 1H); 7.45 (d, J = 8.59 Hz, 2H); 8.14 (d, J = 8.68 Hz, 2H).

General Method B. The following procedure was used to obtain the clobenpropit derivatives **6a**−**l**.

4-(3-Bromopropyl)-1*H*-imidazole hydrobromide (400 mg, 1.48 mmol) and an excess of the corresponding thiourea (500 mg) were dissolved in 3 mL of ethanol in a microwave tube. The reaction mixture was heated in the microwave to 120 °C during 30 min. The ethanol was evaporated, and the residue was purified with flash column chromatography. After the solvents were evaporated, the residue was crystallized from ethanol. The ^{1}H and ^{13}C NMR data are given below, whereas isolated yields, purity by LCMS, and HRMS data are presented in the Supporting Information.

*3-(1H-Imidazol-4-yl)propyl N-Benzyl-N′-cyclopentylcarbamimidothioate (**6a**).* ^{1}H NMR (MeOD, 400 MHz): δ 1.54−1.82 (m, 6H); 1.95−2.21 (m, 4H); 2.78−2.98 (m, 2H); 3.33−3.41 (m, 2H); 4.24 (bs, 1H); 7.33 (s, 1H); 7.39 (bs, 5H); 8.84 (s, 1H). ^{13}C NMR (MeOD, 200 MHz): δ 24.08; 24.52; 24.90; 28.67; 32.96; 34.10; 44.85; 53.35; 57.64; 117.31; 128.19; 128.41; 129.14; 129.53; 130.06 (2C); 133.86; 134.98.

*3-(1H-Imidazol-4-yl)propyl N-Benzyl-N′-cyclohexylcarbamimidothioate (**6b**).* ^{1}H NMR (MeOD, 400 MHz): δ 1.20 (bs, 1H); 1.32−1.51 (m, 4H); 1.63−1.72 (m, 1H); 1.76−1.85 (m, 2H); 1.86−2.09 (m, 4H); 2.65−2.79 (m, 2H); 3.24 (t, J = 7.10 Hz, 2H); 3.73 (bs, 1H); 4.72 (s, 2H); 6.95 (s, 1H); 7.28−7.43 (m, 5H); 7.85 (bs, 1H). ^{13}C NMR (MeOD, 400 MHz): δ 26.18; 26.30; 26.40 (2C); 29.88; 49.40; 55.80; 117.10; 128.92 (3C); 129.69; 130.46 (2C); 136.41; 168.16.

*3-(1H-Imidazol-4-yl)propyl N-Butyl-N′-cyclopentylcarbamimidothioate (**6c**).* ^{1}H NMR (MeOD, 200 MHz): δ 0.97 (t, J = 7.20 Hz, 3H); 1.39 (sx, J_1 = 8.20 Hz, J_2 = 7.10 Hz, J_3 = 7.20 Hz, 2H); 1.57−1.94 (m, 8H); 1.95−2.03 (m, 4H); 2.77 (t, J = 7.10 Hz, 2H); 3.26 (t, J = 7.50 Hz, 2H); 4.08 (bs, 1H); 6.94 (s, 1H); 7.75 (s, 1H). ^{13}C NMR (MeOD, 200 MHz): δ 14.82; 14.89; 21.74; 24.97; 25.30; 25.72; 29.50; 33.62; 33.90; 34.38; 34.72; 42.00; 118.15; 134.69; 135.79.

*3-(1H-Imidazol-4-yl)propyl N-(3,4-Dichlorobenzyl)-N′-cyclohexylcarbamimidothioate (**6d**).* ^{1}H NMR (MeOD, 200 MHz): δ 1.11−1.58 (m, 6H); 1.63−2.12 (m, 6H); 2.71 (t, J = 7.23 Hz, 2H); 3.25 (t, J = 7.06 Hz,2H); 3.76 (bs, 1H); 4.71 (s, 2H); 6.90 (s, 1H); 7.30 (dd, J_1 = 6.15, J_2 = 2.10, 1H); 7.53 (s, 1H); 7.55 (d, J = 8.25 Hz, 1H); 7.73 (s, 1H). ^{13}C NMR (MeOD, 500 MHz): δ 25.94 (2C); 26.03 (2C); 26.12; 29.66; 30.69; 32.85; 61.87; 116.56; 128.41; 130.71; 132.15; 133.10; 133.80 (3C); 136.09; 167.83.

*3-(1H-Imidazol-4-yl)propyl N-(4-Chlorobenzyl)-N′-butylcarbamimidothioate (**6e**).* ^{1}H NMR (MeOD, 400 MHz): δ 0.97 (bs, 3H); 1.25−1.55 (m, 2H); 1.58−1.79 (m, 2H); 2.06 (bs, 2H); 2.83 (bs, 2H); 3.28−3.37 (m, 2H); 3.45−3.52 (m, 2H); 4.71 (bs, 2H), 7.24 (s, 1H); 7.32−7.36 (m, 2H); 7.38−7.43 (m, 2H); 8.51 (s, 1H). ^{13}C NMR (MeOD, 200 MHz): δ 14.03; 20.6; 24.53 (2C); 28.84 (2C); 32.37; 45.62; 117.23; 130.072 (2C); 130.29 (2C); 134.63; 135.21; 168.54.

*3-(1H-Imidazol-4-yl)propyl N-(4-Chlorobenzyl)-N′-benzylcarbamimidothioate (**6f**).* ^{1}H NMR (MeOD, 200 MHz): δ 2.02 (q, J_1 = 7.26 Hz, J_2 = 7.62 Hz, 2H); 2.81 (t, J = 7.56 Hz, 2H); 3.35 (t, J = 7.43 Hz, 2.0H); 4.72 (s, 2H); 4.74 (s, 2H); 7.06−7.55 (m, 10H); 8.64 (s, 1H). ^{13}C NMR (MeOD, 500 MHz): δ 24.13; 28.72; 32.49; 61.44 (2C); 117.20; 129.69 (9C); 134.01 (3C); 134.91; 169.02.

*3-(1H-Imidazol-4-yl)propyl N-(3,4-Dichlorobenzyl)-N′-benzylcarbamimidothioate (**6g**).* ^{1}H NMR (MeOD, 400 MHz)): δ 2.04 (q, J_1 = 6.44 Hz, J_2 = 8044 Hz, 2H); 2.84 (t, J = 7.8 Hz, 2H); 3.40 (t, J = 7.37 Hz, 2H); 4.76 (bs, 4H); 7.11−7.68 (m, 9 h); 8.81 (s, 1H). ^{13}C NMR (MeOD, 400 MHz): δ 24.05; 28.68; 32.51; 43.58; 44.73; 117.24; 127.97; 128.08; 128.41; 128.78; 129.15; 129.46; 130.06; 130.40; 130.84; 131.45; 132.04; 133.70; 133.81; 134.70; 134.88; 169.29.

*3-(1H-Imidazol-4-yl)propyl N-Cyclohexyl-N′-cyclopentylcarbamimidothioate (**6h**).* ^{1}H NMR (400 MHz, MeOD): δ 1.18−1.59 (m, 5H); 1.69 (bs, 5H); 1.82 (bs, 4H); 1.95 (bs, 2H); 2.05−2.15 (m, 4H); 2.93 (t, J = 3.8 Hz, 2H); 3.33−3.39 (m, 2H); 3.84 (bs, 1H); 4.15−4.45 (bs, 1H); 7.45 (s, 1H), 8.88 (s, 1H). ^{13}C NMR (MeOD, 400 MHz): δ 24.22; 24.83; 25.98 (3C); 28.74; 32.98 (5C); 117.36; 133.95; 135.04; 166.29.

*3-(1H-Imidazol-4-yl)propyl N-Cyclopentyl-N′-(tert-butyl)-carbamimidothioate (**6i**).* ^{1}H NMR (MeOD, 400 MHz, T = 330 K): δ 1.52 (s, 9H); 1.62−1.76 (m, 4H); 1.76−1.91 (m, 2H); 2.93 (t, J = 8.0 Hz, 2H); 3.35 (t, J = 8.0 Hz, 2H); 4.30−4.40 (m, 1H), 7.39 (s, 1H); 8.73 (s, 1H). ^{13}C NMR (MeOD, 200 MHz): δ 24.49; 24.88 (2C); 28.85; 29.00; 29.63 (3C); 33.28 (2C); 34.18; 58.17; 117.37; 134.20; 135.04; 167.93.

*3-(1H-Imidazol-4-yl)propyl N-(3,4-Dichlorobenzyl)-N′-butylcarbamimidothioate (**6j**).* ^{1}H NMR (MeOD, 400 MHz): δ 0.87−1.04 (m, 3H); 1.20−1.51 (m, 2H); 1.52−1.79 (m, 2H); 1.99−2.18 (m, 2H); 2.78−2.98 (m, 2H); 3.30−3.46 (m, 2H); 3.53 (t, J = 7.5 Hz, 2H); 4.75 (s, 2H); 7.27−7.43 (m, 2H); 7.55 (d, J = 7.80 Hz, 2H); 8.80 (s, 1H). ^{13}C NMR (MeOD, 400 MHz): δ 14.40; 21.41; 24.62; 29.12; 31.42; 32.94; 46.10; 49.00; 117.72; 128.97 (2C); 132.00; 132.53; 134.16; 134.40; 169.06.

*3-(1H-Imidazol-4-yl)propyl N-(4-Chlorobenzyl)-N′-cyclohexylcarbamimidothioate (**5**).* ^{1}H NMR (MeOD, 200 MHz): δ 1.22 (bs, 1H); 1.31−1.51 (m, 4H); 1.68 (d, J = 12.0 Hz, 1H); 1.82 (d, J = 12.2 Hz, 2H); 1.89−2.12 (m, 4H); 2.80 (t, J = 7.2 Hz, 2H); 3.72−3.79 (m, 1H); 4.72 (s, 2H); 7.25 (s, 1H); 7.34 (d, J = 8.5 Hz, 2H); 7.39 (d, J = 8.5 Hz, 2H); 8.56 (s, 1H). ^{13}C NMR (MeOD, 200 MHz): δ 24.55; 25.87 (2C); 25.93; 28.82; 48.87; 55.20; 117.09; 130.06 (6C); 134.73; 167.59.

*3-(1H-Imidazol-4-yl)propyl N-(4-Cyanobenzyl)-N′-cyclohexylcarbamimidothioate (**6k**).* ^{1}H NMR (MeOD, 500 MHz): δ 1.14−1.60 (m, 5H); 1.68−2.20 (m, 7H); 2.74−3.00 (m, 2H); 3.30−3.45 (m, 2H); 3.82 (s, 1H); 4.86 (s, 2H); 7.38 (s, 1H); 7.57 (d, J = 8.25 Hz, 2H)); 7.77 (d, J = 8.03 Hz, 2H); 8.80 (d, J = 1.23 Hz, 1H). ^{13}C NMR (MeOD, 500 MHz): δ 21.87; 24.10; 25.89; 28.56 (2C); 32.11; 55.74; 61.37; 117.23; 119.27; 129.30; 133.76 (4C); 133.92 (2C); 134.93; 167.72.

*3-(1H-Imidazol-4-yl)propyl N-(4-Nitrobenzyl)-N′-cyclohexylcarbamimidothioate (**6l**).* ^{1}H NMR (MeOD, 500 MHz): δ 1.06−1.62 (m, 5H); 1.7 (bs, 1H); 1.76−2.33 (m, 6H)2.74−3.00 (m, 2H); 3.31−3.56 (m, 2H); 3.85 (s, 1H)7.37 (s, 1H); 7.63 (d, J = 8.78 Hz, 2H); 8.25 (d, J = 8.52 Hz, 2H); 8.79 (s, 1H). ^{13}C NMR (MeOD, 500 MHz): δ 24.19; 25.91; 25.97; 28.66 (2C); 32.73; 55.86; 61.45; 117.30; 124.98 (4C); 129.57; 133.99; 134.16; 134.98; 167.83.

Pharmacology. *DNA Constructs and Site-Directed Mutagenesis.* The wild-type human H_3R and H_4R cDNA (pcDNA3.1) were purchased from the Missouri S & T cDNA Resource Center

(Rollo, MO)/Guthrie cDNA Resource Center (Sayre, PA). The human H_4R cDNA was subcloned into mammalian expression vector pcDEF3 (a gift from Dr. J. Langer) using *Bam*HI and *Xba*I restriction sites. Site-directed mutagenesis was performed with the fusion PCR method using oligonucleotide primers containing the indicated mutations. The mutations were verified by sequence analysis at ServiceXS (Leiden, The Netherlands).

Cell Culture, Transfection, and Membrane Preparation. HEK293T cells were cultured in Dulbecco's modified Eagle medium (DMEM) supplemented with 10% fetal bovine serum (FBS), 50 IU/mL penicillin, and 50 μg/mL streptomycin at 37°C and 5% CO_2. Cells were seeded 2×10^6 per 10 cm dish 1 day prior to transfection. Approximately 4×10^6 cells were transfected with 5 μg of cDNA using the PEI method. Briefly, 5 μg of cDNA was mixed with 20 μg of 25 kDa linear polyethyleneimine in 500 μL of 150 mM NaCl. This transfection mix was incubated at room temperature for 10−30 min and subsequently added dropwise to a 10 cm dish with 6 mL of fresh culture medium. Two days after transfection, transfected cells were washed once with phosphate buffered saline (PBS) and subsequently scraped from their culture dish in 1 mL of PBS. Crude membrane extracts were collected by centrifugation at ∼2000*g* for 10 min at 4°C and stored at −20 °C until further use.

Radioligand Binding Assays. Binding assays were performed using crude membrane extracts from transfected cells in 50 mM Tris-HCl binding buffer (pH 7.4 at room temperature). For heterologous displacement studies, crude membrane extracts were co-incubated with increasing (1 pM to 0.1 mM) concentration of compounds and ∼10 nM [^{3}H]histamine, ∼10 nM [^{3}H]JNJ-7777120 (tritiated **4c**), or ∼1 nM [^{3}H]*N*-α-methylhistamine (NAMH) in a total volume of 100 μL/well. The reaction suspensions were incubated for 1−1.5 h at room temperature on a shaking table (750 rpm). Bound radioligand was separated from free radioligand via rapid filtration over a 0.5% PEI-presoaked glass fiber C plate (GF/C, Perkin-Elmer). GF/C plates were subsequently washed three times with ice-cold 50 mM Tris-HCl wash buffer (pH 7.4 at 4 °C). The retained radioactivity on the GF/C plates was counted by liquid scintillation counting in a Wallac Microbeta (Perkin-Elmer).

Data Analysis. pK_i values were calculated using nonlinear regressions for a single binding site model using GraphPad Prism 4.0. K_d values were previously determined.[12,28]

Materials. [Ring, methylenes-^{3}H(N)]histamine (10−40 Ci/mmol) and *N*-α-[methyl-^{3}H]methylhistamine (45−90 Ci/mmol) were purchased from Perkin-Elmer. [^{3}H]JNJ-7777120 (56.1 Ci/mmol) was a kind gift from R. Thurmond (J&J, La Jolla, CA).

Computational Methods. *Classical QSAR Procedure.* The in silico building, conformational search, and molecular descriptor calculations of **2**, **5**, and **6a−l** were performed using Molecular Operating Environment (MOE) software, version 2006.08, developed by Chemical Computing Group, Inc. (Montreal, Canada) as described previously. The stepwise method from the SPSS 14.0 for Windows was subsequently used to select the important descriptors and generate QSAR models, with the dependent variables being $pK_i(H_3R)$ and $pK_i(H_4R)$.[24,32,51]

3D-QSAR Procedure. The structures and the major protonation states of compounds **2**, **5**, and **6a−l** at pH 7.4 were built and determined using MarvinSketch, version 5.2.5.1, from ChemAxon.[52] The 3D structure of compound **6** was subsequently generated using CORINA 3.46, resulting in two 3D configurations.[34] Ab initio optimizations using DFT/6-31G* by employing the Gaussian 03 software package were performed to both 3D configurations.[35−37] The lower energy configuration suggested by the ab initio calculation was selected as the reference 3D structure to align protonated **1** and **7a−l** by using OMEGA, version 2.3.2, and ROCS, version 2.3.1.[38,39] The alignment was refined subsequently using MOE, version 2009.10.[32] The MIF probes (DRY, N1, O, and O::) were then calculated using the GRID package, version 22.0.3, from Molecular Discovery.[26,53] The probes in a radius of 5 Å around aligned compounds were calculated using a grid resolution of 1 Å. The probes values were normalized, and probes with standard deviation of less than 1.0 were filtered out by employing R statistical package, version 2.7.1.[54] The GreedyStepwise method from the Weka 3.6.2 data-mining software package followed by the stepwise method from the SPSS 14.0 for Windows was subsequently used to select the important probes and generate QSAR models, with the dependent variables being $pK_i(H_3R)$ and $pK_i(H_4R)$.[24,32,51]

Homology Modeling Procedure. The H_4R model was constructed as previously described.[28] Very recently, during the preparation of the current paper, the doxepin-bound crystal structure of the histamine H_1 receptor was published. A preliminary H_4R homology model made based on this H_1R crystal structure is very similar to the H_4R model used in the current study, which is derived from the ADRB2 crystal structure[41] (data not shown). This is in line with the fact that the H_1R and ADRB2 crystal structures have a similar structure (Supporting Information Figure 2).[53] Compound **6** was docked into the H_4R receptor model without constraint using PLANTS.[55] The first pose showing adjacency between the imidazole moiety and $E^{5.46}$ was subjected to energy minimization in MOE, version 2009.10,[32] using restrained H-bonds between the protonated imidazole nitrogen atom of the ligand and one of the carboxylate oxygen atoms (OE2) of $E^{5.46}$ and between the protonated isothiourea moiety of the ligand and one of the carboxylate oxygen atoms (OD2) of $D^{3.32}$ (model **6A**, Figure 3C). On the other hand, the first pose showing adjacency between the imidazole moiety and $D^{3.32}$ was subjected to energy minimization in MOE, version 2009.10,[32] using restrained H-bonds between the protonated imidazole nitrogen atom of the ligand and one of the carboxylate oxygen atoms (OD2) of $D^{3.32}$ and between the protonated isothiourea moiety of the ligand and one of the carboxylate oxygen atoms (OE2) of $E^{5.46}$ (model **6B**, Figure 3D). Compound **1** was docked without constraint into model **6A**.[55] The first ranked pose was subjected to energy minimization in MOE, version 2009.10,[32] using restrained H-bonds between the protonated imidazole nitrogen atom of the ligand and one of the carboxylate oxygen atoms (OE2) of $E^{5.46}$ and between the protonated isothiourea moiety of the ligand and one of the carboxylate oxygen atoms (OD2) of $D^{3.32}$ (model **1A**, Figure 3A). Compound **1** was also docked without constraint into the model **6B**.[55] The first ranked pose was subjected to energy minimization in MOE, version 2009.10,[32] using restrained H-bonds between the protonated imidazole nitrogen atom of the ligand and one of the carboxylate oxygen atoms (OD2) of $D^{3.32}$ and between the protonated isothiourea moiety of the ligand and one of the carboxylate oxygen atoms (OE2) of $E^{5.46}$ (model **1B**, Figure 3B).

Molecular Dynamics Procedure. The models **1A**, **1B**, **6A**, and **6B** were then minimized using AMBER 10 to relax the structure.[56] Force-field parameters for the ligands were derived using the Antechamber program, and partial charges for the ligands were computed using the AM1-BCC procedure in Antechamber.[56] Upper-bound distance restraint of 3.5 Å to maintain the interaction of the ligand to $D^{3.32}$ 3.5 Å was applied. The minimized model was subsequently embedded in a pre-equilibrated lipid bilayer consisting of molecules of 1-palmitoyl-2-oleoylphosphatidylcholine (POPC) and solvated with TIP3P water molecules (box dimensions of 79.2 Å × 72.0 Å × 76.9 Å) as described by Urizar et al.[57] The complexes embedded in the hydrated lipid bilayer were minimized shortly using AMBER 10.[56] The hydrogen bond to $D^{3.32}$ constraint and a positional harmonic constraint of 50 kcal mol^{-1} $Å^{-1}$ on Cα carbon atoms were applied. The entire system was then subjected to a 1.1 ns constant pressure molecular dynamics (MD) simulation. All bonds involving hydrogen atoms were frozen with the SHAKE algorithm. During the first 100 ps, the Cα carbon atoms were constrained and the hydrogen bond of the ligand to $D^{3.32}$ was restrained as previously described and the temperature was linearly increased from 0 to 300 K. During the last 1000 ps, the temperature was kept constant at 300 K and the pressure at 1 bar, using a coupling constant of 0.2 ps and the Berendsen approach. Interactions were calculated according to the AMBER 03 force field, using particle-mesh-Ewald (PME) summation to include the long-range electrostratic forces. van der Waals interactions were calculated using a cutoff of 8.0 Å. MD snapshots were extracted at every 1 ps.[58,59] This yielded 1000 snapshot for each model. The binding pocket regions of MD snapshots were then fitted to the corresponding binding pocket regions of the initial 3D model. The

interaction fingerprint (IFP) for each snapshot was calculated subsequently.[60] Snapshots with hydrogen bond to $D^{3.32}$ were counted.

■ ASSOCIATED CONTENT

Supporting Information

Purity and HRMS data for compounds **2**, **5**, and **6a−l** as determined by LCMS; alignment of compounds **2**, **5**, and **6a−l** used in 3D-QSAR and the values of the most influential descriptors in eqs 1-5; analysis of H_4R-ligand H-bond interactions MD simulations; comparison of ligand binding modes in ADRB2 and H_1R crystal structures and H_4R models. This material is available free of charge via the Internet at http://pubs.acs.org.

■ AUTHOR INFORMATION

Corresponding Author

*Phone: +31(0)205987553. Fax: +31(0)205987610. E-mail: C.de.Graaf@vu.nl.

Author Contributions

[§]These authors contributed equally.

■ ACKNOWLEDGMENTS

This work was supported by the Top Institute Pharma [Project Number D1.105: The GPCR Forum], The Netherlands Organization for Scientific Research [NWO VENI Grant 700.59.408], and COST Action BM0806. Sven Uleman is acknowledged for technical assistance.

■ ABBREVIATIONS USED

3D-QSAR, three-dimensional quantitative structure−activity relationship; ADRB1, β_1-adrenergic; ADRB2, β_2-adrenergic; DRD3, dopamine D3; GPCR, G protein-coupled receptor; H_1R, histamine H_1 receptor; H_3R, histamine H_3 receptor; H_4R, histamine H_4 receptor; SDM, site-directed mutagenesis

■ ADDITIONAL NOTE

During the preparation of this manuscript, a crystal structure of the human histamine H_1 receptor (H_1R) was solved (PDB code 3RZE, released June 15, 2011) by Iwata et al. (*Nature* 2011, *475*, 65−70). The overallstructure of H_1R is shown to be similar to the β_2-adrenergic (ADRB2) crystal structure. As a result, H_4R models based on the new H_1R crystal structure are very similar to the ADRB2-based H_4R models described in the current study (C. de Graaf, unpublished results).

■ REFERENCES

(1) Istyastono, E. P.; de Graaf, C.; de Esch, I. J. P.; Leurs, R. Molecular determinants of selective agonist and antagonist binding to the histamine H_4 receptor. *Curr. Top. Med. Chem.* **2011**, *11*, 661−679.

(2) Liu, C.; Ma, X.; Jiang, X.; Wilson, S. J.; Hofstra, C. L.; Blevitt, J.; Pyati, J.; Li, X.; Chai, W.; Carruthers, N.; Lovenberg, T. W. Cloning and pharmacological characterization of a fourth histamine receptor (H(4)) expressed in bone marrow. *Mol. Pharmacol.* **2001**, *59*, 420−426.

(3) Smits, R. A.; Leurs, R.; de Esch, I. J. Major advances in the development of histamine H_4 receptor ligands. *Drug Discovery Today* **2009**, *14*, 745−753.

(4) Thurmond, R. L.; Gelfand, E. W.; Dunford, P. J. The role of histamine H_1 and H_4 receptors in allergic inflammation: the search for new antihistamines. *Nat. Rev. Drug Discovery* **2008**, *7*, 41−53.

(5) Zampeli, E.; Tiligada, E. The role of histamine H_4 receptor in immune and inflammatory disorders. *Br. J. Pharmacol.* **2009**, *157*, 24−33.

(6) Lim, H. D.; van Rijn, R. M.; Ling, P.; Bakker, R. A.; Thurmond, R. L.; Leurs, R. Evaluation of histamine H_1-, H_2-, and H_3-receptor ligands at the human histamine H_4 receptor: identification of 4-methylhistamine as the first potent and selective H_4 receptor agonist. *J. Pharmacol. Exp. Ther.* **2005**, *314*, 1310−1321.

(7) Liu, C.; Wilson, S. J.; Kuei, C.; Lovenberg, T. W. Comparison of human, mouse, rat, and guinea pig histamine H_4 receptors reveals substantial pharmacological species variation. *J. Pharmacol. Exp. Ther.* **2001**, *299*, 121−130.

(8) Nguyen, T.; Shapiro, D. A.; George, S. R.; Setola, V.; Lee, D. K.; Cheng, R.; Rauser, L.; Lee, S. P.; Lynch, K. R.; Roth, B. L.; O'Dowd, B. F. Discovery of a novel member of the histamine receptor family. *Mol. Pharmacol.* **2001**, *59*, 427−433.

(9) Oda, T.; Morikawa, N.; Saito, Y.; Masuho, Y.; Matsumoto, S. Molecular cloning and characterization of a novel type of histamine receptor preferentially expressed in leukocytes. *J. Biol. Chem.* **2000**, *275*, 36781−367816.

(10) Gemkow, M. J.; Davenport, A. J.; Harich, S.; Ellenbroek, B. A.; Cesura, A.; Hallett, D. The histamine H_3 receptor as a therapeutic drug target for CNS disorders. *Drug Discovery Today* **2009**, *14*, 509−515.

(11) Uveges, A. J.; Kowal, D.; Zhang, Y.; Spangler, T. B.; Dunlop, J.; Semus, S.; Jones, P. G. The role of transmembrane helix **5** in agonist binding to the human H_3 receptor. *J. Pharmacol. Exp. Ther.* **2002**, *301*, 451−459.

(12) Jongejan, A.; Lim, H. D.; Smits, R. A.; de Esch, I. J.; Haaksma, E.; Leurs, R. Delineation of agonist binding to the human histamine H_4 receptor using mutational analysis, homology modeling, and ab initio calculations. *J. Chem. Inf. Model.* **2008**, *48*, 1455−1463.

(13) Ishikawa, M.; Watanabe, T.; Kudo, T.; Yokoyama, F.; Yamauchi, M.; Kato, K.; Kakui, N.; Sato, Y. Investigation of the histamine H_3 receptor binding site. Design and synthesis of hybrid agonists with a lipophilic side chain. *J. Med. Chem.* **2010**, *53*, 6445−6456.

(14) Kiss, R.; Noszal, B.; Racz, A.; Falus, A.; Eros, D.; Keseru, G. M. Binding mode analysis and enrichment studies on homology models of the human histamine H_4 receptor. *Eur. J. Med. Chem.* **2008**, *43*, 1059−1070.

(15) Lorenzi, S.; Mor, M.; Bordi, F.; Rivara, S.; Rivara, M.; Morini, G.; Bertoni, S.; Ballabeni, V.; Barocelli, E.; Plazzi, P. V. Validation of a histamine H_3 receptor model through structure−activity relationships for classical H_3 antagonists. *Bioorg. Med. Chem.* **2005**, *13*, 5647−5657.

(16) Schlegel, B.; Laggner, C.; Meier, R.; Langer, T.; Schnell, D.; Seifert, R.; Stark, H.; Holtje, H. D.; Sippl, W. Generation of a homology model of the human histamine H_3 receptor for ligand docking and pharmacophore-based screening. *J. Comput.-Aided Mol. Des.* **2007**, *21*, 437−453.

(17) Rai, B. K.; Tawa, G. J.; Katz, A. H.; Humblet, C. Modeling G protein-coupled receptors for structure-based drug discovery using low-frequency normal modes for refinement of homology models: application to H_3 antagonists. *Proteins* **2009**, *78*, 457−473.

(18) Wijtmans, M.; de Graaf, C.; de Kloe, G.; Istyastono, E. P.; Smit, J.; Lim, H.; Boonnak, R.; Nijmeijer, S.; Smits, R. A.; Jongejan, A.; Zuiderveld, O.; de Esch, I. J.; Leurs, R. Triazole ligands reveal distinct molecular features that induce histamine H_4 receptor affinity and subtly govern H_4/H_3 subtype selectivity. *J. Med. Chem.* **2011**, *54*, 1693−1703.

(19) Cherezov, V.; Rosenbaum, D. M.; Hanson, M. A.; Rasmussen, S. G.; Thian, F. S.; Kobilka, T. S.; Choi, H. J.; Kuhn, P.; Weis, W. I.; Kobilka, B. K.; Stevens, R. C. High-resolution crystal structure of an engineered human β_2-adrenergic G protein-coupled receptor. *Science* **2007**, *318*, 1258−1265.

(20) Chien, E. Y.; Liu, W.; Zhao, Q.; Katritch, V.; Han, G. W.; Hanson, M. A.; Shi, L.; Newman, A. H.; Javitch, J. A.; Cherezov, V.; Stevens, R. C. Structure of the human dopamine D3 receptor in complex with a D2/D3 selective antagonist. *Science* **2010**, *330*, 1091−1095.

(21) Shimamura, T.; Shiroishi, M.; Weyand, S.; Tsujimoto, H.; Winter, G.; Katritch, V.; Abagyan, R.; Cherezov, V.; Liu, W.; Han, G. W.; Kobayashi, T.; Stevens, R. C.; Iwata, S. Structure of the human

histamine H_1 receptor complex with doxepin. *Nature* **2011**, *475*, 65−70.
(22) Warne, T.; Serrano-Vega, M. J.; Baker, J. G.; Moukhametzianov, R.; Edwards, P. C.; Henderson, R.; Leslie, A. G.; Tate, C. G.; Schertler, G. F. Structure of a β_1-adrenergic G-protein-coupled receptor. *Nature* **2008**, *454*, 486−491.
(23) de Graaf, C.; Rognan, D. Customizing G protein-coupled receptor models for structure-based virtual screening. *Curr. Pharm. Des.* **2009**, *15*, 4026−4048.
(24) Lim, H. D.; Istyastono, E. P.; van de Stolpe, A.; Romeo, G.; Gobbi, S.; Schepers, M.; Lahaye, R.; Menge, W. M.; Zuiderveld, O. P.; Jongejan, A.; Smits, R. A.; Bakker, R. A.; Haaksma, E. E.; Leurs, R.; de Esch, I. J. Clobenpropit analogs as dual activity ligands for the histamine H_3 and H_4 receptors: synthesis, pharmacological evaluation, and cross-target QSAR studies. *Bioorg. Med. Chem.* **2009**, *17*, 3987−3994.
(25) De Esch, I. J.; Mills, J. E.; Perkins, T. D.; Romeo, G.; Hoffmann, M.; Wieland, K.; Leurs, R.; Menge, W. M.; Nederkoorn, P. H.; Dean, P. M.; Timmerman, H. Development of a pharmacophore model for histamine H_3 receptor antagonists, using the newly developed molecular modeling program SLATE. *J. Med. Chem.* **2001**, *44*, 1666−1674.
(26) Dezi, C.; Carotti, A.; Magnani, M.; Baroni, M.; Padova, A.; Cruciani, G.; Macchiarulo, A.; Pellicciari, R. Molecular interaction fields and 3D-QSAR studies of p53-MDM2 inhibitors suggest additional features of ligand−target interaction. *J. Chem. Inf. Model.* **2010**, *50*, 1451−1465.
(27) Lim, H. D.; Jongejan, A.; Bakker, R. A.; Haaksma, E.; de Esch, I. J.; Leurs, R. Phenylalanine 169 in the second extracellular loop of the human histamine H_4 receptor is responsible for the difference in agonist binding between human and mouse H_4 receptors. *J. Pharmacol. Exp. Ther.* **2008**, *327*, 88−96.
(28) Lim, H. D.; de Graaf, C.; Jiang, W.; Sadek, P.; McGovern, P. M.; Istyastono, E. P.; Bakker, R. A.; de Esch, I. J.; Thurmond, R. L.; Leurs, R. Molecular determinants of ligand binding to H_4R species variants. *Mol. Pharmacol.* **2010**, *77*, 734−743.
(29) Bloemhoff, W.; Kerling, K. *Recl. Trav. Chim. Pays-Bas* **1970**, *89*, 1181.
(30) Kivits, G. A. A.; Hora, J. A convenient preparation of 3-(1*H*-imidazol-4-yl)propanol. *J. Heterocycl. Chem.* **1975**, *12*, 577.
(31) Wildman, S. A.; Crippen, G. M. Prediction of physiochemical parameters by atomic contributions. *J. Chem. Inf. Comput. Sci.* **1999**, *39*, 868−873.
(32) *MOE*, version 2009.10; Chemical Computing Group (CCG): Montreal, Canada, 2009; http://www.chemcomp.com/software.htm:.
(33) Muzammil, S.; Armstrong, A. A.; Kang, L. W.; Jakalian, A.; Bonneau, P. R.; Schmelmer, V.; Amzel, L. M.; Freire, E. Unique thermodynamic response of tipranavir to human immunodeficiency virus type 1 protease drug resistance mutations. *J. Virol.* **2007**, *81*, 5144−5154.
(34) Sadowski, J.; Gasteiger, J.; Klebe, G. Comparison of automatic three-dimensional model builders using 639 X-ray structures. *J. Chem. Inf. Comput. Sci.* **1994**, *34*, 1000−1008.
(35) Iqbal, P.; Patel, D. S.; Bharatam, P. V. Ab initio study on *N*,*N*2,*N*3-triaminoguanidine. *J. Phys. Org. Chem.* **2007**, *20*, 1072−1080.
(36) Netzeva, T. I.; Aptula, A. O.; Benfenati, E.; Cronin, M. T.; Gini, G.; Lessigiarska, I.; Maran, U.; Vracko, M.; Schuurmann, G. Description of the electronic structure of organic chemicals using semiempirical and ab initio methods for development of toxicological QSARs. *J. Chem. Inf. Model.* **2005**, *45*, 106−114.
(37) Frisch, M. J.; Trucks, G. W.; Schlegel, H. B.; Scuseria, G. E.; Robb, M. A.; Cheeseman, J. R.; Montgomery, J. A., Jr.; Vreven, T.; Kudin, K. N.; Burant, J. C.; Millam, J. M.; Iyengar, S. S.; Tomasi, J.; Barone, V.; Mennucci, B.; Cossi, M.; Scalmani, G.; Rega, N.; Petersson, G. A.; Nakatsuji, H.; Hada, M.; Ehara, M.; Toyota, K.; Fukuda, R.; Hasegawa, J.; Ishida, M.; Nakajima, T.; Honda, Y.; Kitao, O.; Nakai, H.; Klene, M.; Li, X.; Knox, J. E.; Hratchian, H. P.; Cross, J. B.; Bakken, V.; Adamo, C.; Jaramillo, J.; Gomperts, R.; Stratmann, R. E.; Yazyev, O.; Austin, A. J.; Cammi, R.; Pomelli, C.; Ochterski, J. W.; Ayala, P. Y.; Morokuma, K.; Voth, G. A.; Salvador, P.; Dannenberg, J. J.; Zakrzewski, V. G.; Dapprich, S.; Daniels, A. D.; Strain, M. C.; Farkas, O.; Malick, D. K.; Rabuck, A. D.; Raghavachari, K.; Foresman, J. B.; Ortiz, J. V.; Cui, Q.; Baboul, A. G.; Clifford, S.; Cioslowski, J.; Stefanov, B. B.; Liu, G.; Liashenko, A.; Piskorz, P.; Komaromi, I.; Martin, R. L.; Fox, D. J.; Keith, T.; Al-Laham, M. A.; Peng, C. Y.; Nanayakkara, A.; Challacombe, M.; Gill, P. M. W.; Johnson, B.; Chen, W.; Wong, M. W.; Gonzalez, C.; Pople, J. A. *Gaussian 03*; Gaussian Inc.: Pittsburgh, PA, 2003.
(38) *ROCS*, version 2.3.1; OpenEye Scientific Software Inc.: Santa Fe, NM , 2009; http://www.eyesopen.com.
(39) *OMEGA*, version 2.3.2; OpenEye Scientific Software Inc.: Santa Fe, NM, 2008; http://www.eyesopen.com.
(40) Eriksson, L.; Jaworska, J.; Worth, A. P.; Cronin, M. T.; McDowell, R. M.; Gramatica, P. Methods for reliability and uncertainty assessment and for applicability evaluations of classification- and regression-based QSARs. *Environ. Health Perspect.* **2003**, *111*, 1361−1375.
(41) Rucker, C.; Rucker, G.; Meringer, M. *y*-Randomization and its variants in QSPR/QSAR. *J. Chem. Inf. Model.* **2007**, *47*, 2345−2357.
(42) Shin, N.; Coates, E.; Murgolo, N. J.; Morse, K. L.; Bayne, M.; Strader, C. D.; Monsma, F. J. Jr. Molecular modeling and site-specific mutagenesis of the histamine-binding site of the histamine H_4 receptor. *Mol. Pharmacol.* **2002**, *62*, 38−47.
(43) Wu, B.; Chien, E. Y.; Mol, C. D.; Fenalti, G.; Liu, W.; Katritch, V.; Abagyan, R.; Brooun, A.; Wells, P.; Bi, F. C.; Hamel, D. J.; Kuhn, P.; Handel, T. M.; Cherezov, V.; Stevens, R. C. Structures of the CXCR4 chemokine GPCR with small-molecule and cyclic peptide antagonists. *Science* **2010**, *330*, 1066−1071.
(44) Scholten, D. J.; Canals, M.; Maussang, D.; Roumen, L.; Smit, M. J.; Wijtmans, M.; de Graaf, C.; Vischer, H. F.; Leurs, R. Pharmacological modulation of chemokine receptor function. *Br. J. Pharmacol.* [Online early access]. DOI: 10.1111/j.1476-5381.2011.01551.x. Published Online: Jun 23, **2011**.
(45) Kufareva, I.; Rueda, M.; Katritch, V.; Stevens, R. C.; Abagyan, R. Status of GPCR modeling and docking as reflected by community-wide GPCR Dock 2010 assessment. *Structure* **2011**, *19*, 1108−1126.
(46) Roumen, L.; Sanders, M. P. A.; Vroling, B.; de Esch, I. J. P.; De Vlieg, J.; Leurs, R.; Klomp, J.; Nabuurs, S. B.; de Graaf, C. In silico veritas: the pitfalls and challenges of predicting GPCR−ligand interactions. *Pharmaceuticals* **2011**, *4*, 1196−1215.
(47) Leurs, R.; Chazot, P. L.; Shenton, F. C.; Lim, H. D.; de Esch, I. J. Molecular and biochemical pharmacology of the histamine H_4 receptor. *Br. J. Pharmacol.* **2009**, *157*, 14−23.
(48) Sansuk, K.; Deupi, X.; Torrecillas, I. R.; Jongejan, A.; Nijmeijer, S.; Bakker, R. A.; Pardo, L.; Leurs, R. A structural insight into the reorientation of transmembrane domains 3 and 5 during family A G protein-coupled receptor activation. *Mol. Pharmacol.* **2011**, *79*, 262−9.
(49) Schnell, D.; Strasser, A.; Seifert, R. Comparison of the pharmacological properties of human and rat histamine H_3-receptors. *Biochem. Pharmacol.* **2010**, *80*, 1437−1449.
(50) Yao, B. B.; Hutchins, C. W.; Carr, T. L.; Cassar, S.; Masters, J. N.; Bennani, Y. L.; Esbenshade, T. A.; Hancock, A. A. Molecular modeling and pharmacological analysis of species-related histamine H(3) receptor heterogeneity. *Neuropharmacology* **2003**, *44*, 773−786.
(51) *SPSS 14.0 for Windows*; SPSS Inc.: Chicago, IL, 2005; http://spss.com/.
(52) *MarvinSketch*, version 5.2.5.1; ChemAxon: Budapest, Hungary, 2009.
(53) Goodford, P. J. A computational procedure for determining energetically favorable binding sites on biologically important macromolecules. *J. Med. Chem.* **1985**, *28*, 849−857.
(54) *R: A Language and Environment for Statistical Computing*; R Development Core Team: Vienna, Austria, 2008; http://www.R-project.org.
(55) Korb, O.; Stützle, T.; Exner, T. E. Empirical scoring functions for advanced protein−ligand docking with PLANTS. *J. Chem. Inf. Model.* **2009**, *49*, 84−96.

(56) Case, D. A.; Darden, T. A.; Cheatham, T. E., III; Simmerling, C. L.; Wang, J.; Duke, R. E.; Luo, R.; Crowley, M.; Walker, R. C.; Zhang, W.; Merz, K. M.; Wang, B.; Hayik, S.; Roitberg, A.; Seabra, G.; Kolossváry, I.; Wong, K. F.; Paesani, F.; Vanicek, J.; Wu, X.; Brozell, S. R.; Steinbrecher, T.; Gohlke, H.; Yang, L.; Tan, C.; Mongan, J.; Hornak, V.; Cui, G.; Mathews, D. H.; Seetin, M. G.; Sagui, C.; Babin, V.; Kollman, P. A. *AMBER 10*, University of California: San Francisco, 2008.

(57) Urizar, E.; Claeysen, S.; Deupi, X.; Govaerts, C.; Costagliola, S.; Vassart, G.; Pardo, L. An activation switch in the rhodopsin family of G protein-coupled receptors: the thyrotropin receptor. *J. Biol. Chem.* **2005**, *280*, 17135−17141.

(58) de Graaf, C.; Foata, N.; Engkvist, O.; Rognan, D. Molecular modeling of the second extracellular loop of G-protein coupled receptors and its implication on structure-based virtual screening. *Proteins* **2008**, *71*, 599−620.

(59) Van Der Spoel, D.; Lindahl, E.; Hess, B.; Groenhof, G.; Mark, A. E.; Berendsen, H. J. GROMACS: fast, flexible, and free. *J. Comput. Chem.* **2005**, *26*, 1701−1718.

(60) Marcou, G.; Rognan, D. Optimizing fragment and scaffold docking by use of molecular interaction fingerprints. *J. Chem. Inf. Model.* **2007**, *47*, 195−207.

(61) Stanton, D. T. Evaluation and use of BCUT Descriptors in QSAR and QSPR studies. *J. Chem. Inf. Comput. Sci.* **1999**, *39*, 11−20.